Neutron resonance spectroscopy for $n+{}^{52}$Cr: Total and differential elastic scattering cross sections

R. F. Carlton

Physics & Astronomy Department, Middle Tennessee State University, Murfreesboro, Tennessee 37132

J. A. Harvey, D. C. Larson, and N. W. Hill

Oak Ridge National Laboratory, Oak Ridge, Tennessee 37831

Neutron total and elastic scattering cross sections have been measured over the neutron energy range 0.040–1.55 MeV. Spins and parities have been deduced for 90% of the resonances observed in the $n+{}^{52}$Cr reaction up to 1.05 MeV. This work brings into doubt a previously claimed parity dependence of the level spacing in ^{53}Cr. We have used an R-matrix analysis to obtain resonance parameters for 194 resonances up to 1.05 MeV and strengths and level spacings for partial waves up to and including $d_{5/2}$. The conventional s-, p-, and d-wave strength functions have been determined to be 3.5 ± 1.0, 0.44 ± 0.08, and 2.9 ± 0.4, respectively (in units of 10^{-4}). This is the first work to report d-wave strength in this nuclide, identifying 87 additional resonances in this group. This, in turn, has resulted in a significant increase in the p-wave level spacing compared to that of two other similar works. Evidence is presented to explain differences among evaluated nuclear data files for this nuclide in terms of the influence of the strength outside the region upon the background cross section.

PACS number(s): 24.30.Gd, 25.40.Dn, 27.40.+z, 29.30.Hs

I. INTRODUCTION

The number of past investigations of neutron interactions with ^{52}Cr is, from a practical standpoint, related to its presence in structural components of nuclear reactors. From a theoretical standpoint this nuclide is of interest due to the magic number of neutrons in the nucleus. These studies have included capture cross section [1], transmission [2,3], elastic and inelastic-scattering measurements [4], and combinations thereof [5,6]. Each of these provides characteristic and often unique information on the interaction process between neutron and target nucleus. Capture measurements provide nuclear level information derived from narrow resonances that are often unobservable in transmission measurements. The R-matrix fitting of total cross-section data deduced from transmission measurements yields resonance parameters and average structure properties, such as strength functions and the external R functions. In favorable cases these total cross sections may be the arbiter of spin (J) assignments through the peak cross section of the resonance. Elastic-scattering measurements are well suited to the determination of the parity of a resonance through the unambiguous asymmetry differences manifested in the elastic scattering cross sections at forward and backward angles and of the spin of a resonance through differences in peak height. Inelastic-scattering cross sections often provide spin and parity information for excited states of the target nucleus.

Past capture measurements have been restricted, by resolution limitations, to energies less than approximately 500 keV. Capture is a sensitive probe at low neutron energies, often revealing resonances that are not detected in transmission studies. In the case of ^{52}Cr, for example, only 19 of the 36 resonances seen below 200 keV in one capture study are also seen in transmission studies [6], whereas between 200 and 500 keV, 50 of the 59 resonances observed in transmission are also seen in capture. Transmission measurements on

^{52}Cr have been analyzed [3,6] up to a neutron energy of 1 MeV. As many as 200 resonances have been observed [6] and strength functions and level spacings have been deduced for s- and p-wave interactions with the ^{52}Cr nucleus. Total and integrated elastic and inelastic-scattering cross sections, taken from numerous data sets over the neutron energy range 1–9 MeV, have been used [4] to explore the optical model potential for this nuclide and deduce model parameters.

The first capture- and transmission-study probed the $n+{}^{52}$Cr interaction up to approximately 250 keV neutron energy [5]. Later the energy range of transmission measurements was extended [3] to 900 keV with the increased resolution afforded by the 80-m flight path of the Oak Ridge Electron Linear Accelerator (ORELA). These data were analyzed using a multilevel R-matrix formalism to deduce neutron energies, neutron widths, and spin and parity assignments. Without the aid of complementary scattering measurements, however, the assignment of J^{π} values on the basis of resonance asymmetry alone can be highly subject to misassignment. There is no evidence that the use of resonance asymmetry, as a basis for J^{π} determination in that study [3], included any sources other than the resonance-potential scattering interference as dictated by the interaction radius assumed in the analysis. This can result in an incorrect assessment, especially near regions of enhanced neutron strength of a particular J component. For example, since ^{52}Cr is near the $3s$ size resonance, there clearly will be s-wave strength above the neutron energy range of the analysis. It has been well established [7] that this external strength results in an additional contribution to the resonance-potential scattering interference for that partial-wave component. This can be modeled through fictitious *dummy* resonances or through a logarithmic formulation as discussed in Sec. III. Except for s-wave resonances, spin and parity as-

signments that are based upon observed resonance asymmetries in transmission alone are thus highly suspect, especially when ignoring the influence of such external strengths.

Parity dependences of the level densities have been discussed [3], the above caveat notwithstanding. The most recent transmission study [6] included measurements at four different flight paths at the Geel linac facility. This study also included capture measurements up to 500 keV, but only nominally increased the energy range in the transmission measurements. Since the flight path used was substantially greater (up to 400 m vs 80 m) the number of analyzed resonances was increased from 133 to 200. The focus of that study included a determination of whether or not the resonance parameters will have nonstatistical properties as expected on the basis of the magic number of neutrons in ^{52}Cr and as suggested by reports of a strong correlation between neutron and radiative widths observed in capture and transmission measurements. There, as in the previous transmission study, spin assignments were established on the basis of asymmetries resulting from interference between resonance and potential scattering. Even with the increased resolution of the 400-m data this is not a sound basis for assigning spins and parities, especially for small resonances.

The presence of chromium in any advanced structural components envisioned for future reactors accentuates the need of accurate assessments of neutron interactions therewith. Salvatores [8], in highlighting the need for a better measure of the interaction, showed dispersions of the average total cross section of ^{52}Cr among the Evaluated Nuclear Data Files (ENDF/B-6), the Joint European Files (JEF-2), and the Japanese Evaluated Nuclear Data Library (JENDL-3) data files of as much as 1 b and 0.5 b for neutron energy ranges of 1–100 keV and 100–1000 keV, respectively. Subgroup II of the NEANSC Working Group on International Evaluation Cooperation has indicated [9] that the dispersion is in part a consequence of the use of different nuclear radii and *dummy* resonances for different energy regions. Other possible reasons, suggested by the present work, are discussed in Sec. IV.

The present study combines transmission and elastic-scattering measurements, both taken at the 200-m flight path of the ORELA facility, for a more thorough assessment of the spins and parities of the individual resonances. In addition, resonance parameters have been extracted to obtain the strength functions and level spacings for individual partial wave components up to and including $d_{5/2}$, this in a fashion that incorporates global external or *dummy* influences with the same nuclear radius for all partial waves. Past studies have assumed or concluded that only s- and p-wave properties need be considered, despite the expectation that d-wave interaction is likely to be significant when the s-wave interaction is large. Concomitantly, the p wave is expected to be smaller in strength under these conditions. Because we are able to deduce the partial wave contributions to the total cross section using both resonance asymmetries in the total cross section and in the elastic-scattering cross section for a series of forward and backward angles, we are able to also calculate energy averaged scattering functions for individual partial wave components. These can then be used, through

comparisons to predictions of an optical model, to determine optical potential well parameters. This will be the focus of a future paper.

II. EXPERIMENT

We have performed transmission and elastic scattering measurements by the time-of-flight technique, using neutron pulses from the ORELA, at a flight path of 201.575 ± 0.005 m, for a target of ^{52}Cr. The neutron burst has a continuous energy spectrum produced by the photoneutron process in tantalum. The neutron energy resolution function is dominated by the burst width (6 ns) and the full width at half maximum is given by

$$\left(\frac{dE}{E}\right)^2 = 0.64E(\text{MeV}) \times 10^{-6}, \tag{1}$$

where E is in MeV.

A. Transmission

The 140-MeV electron beam burst width was 6.0 ns and the accelerator was pulsed at 575 bursts per second at a power level of approximately 4 kW. Collimators were used to focus on the unmoderated neutrons from the Ta target. Overlap neutrons were eliminated by a 0.3-g/cm^2 ^{10}B filter. The intensity of the gamma flash from the Ta target was reduced by 3.7 cm of uranium positioned 5 m from the target. The 42.135 ± 0.050 g sample of 99.87% ^{52}Cr in the form of ^{52}Cr$_2$O$_3$ was 2.65 cm in diameter, corresponding to an inverse thickness of 17.0 b/atom. Other isotopes of chromium in the sample included 0.01, 0.12, and 0.01 % of ^{50}Cr, ^{53}Cr, and ^{54}Cr, respectively. In attempting to avoid the problematic correction for ^{16}O contributions to the measured transmissions we employed O compensation by alternate cycling in and out of the neutron beam of the samples of ^{52}Cr$_2$O$_3$ + Be and a sample of BeO whose thickness was intended to be identical to that of the oxide portion of the ^{52}Cr sample. As discussed in Sec. III A this compensation was found to be less than perfect due possibly to water absorption. Though not serious this could, if not corrected, have diminished the confidence of deduced neutron widths and J^π assignments in the energy region of large oxygen resonances. These samples were positioned 9 m from the neutron target where the neutron beam was collimated to a diameter of 2.38 cm. The samples were cycled in and out of the neutron beam under computer control with a cycle time of approximately 20 min and 14 min, respectively, per sample. We used a neutron monitor to compensate for fluctuations in the neutron production rate during the three week interval and a total of 265 hours of data collection. The six individual runs were added to form the final data set which was then corrected for dead time and background contributions.

Neutrons were detected 192.575 m downstream from the sample by a proton recoil detector in which the neutrons traversed a 2.54 cm thickness of a 5.2 cm by 8.9 cm piece of NE110. The plastic scintillator was optically coupled between two RCA 8854 photomultiplier tubes. Approximately 70% of the neutrons interacted with the target and the re-

maining 30% were transmitted through the detector without producing a proton recoil. Additional information concerning the data acquisition has been reported in detail elsewhere [10]. The data were corrected only for a constant background. A discussion of these and other experimental details may be found elsewhere [11]. The transmission was then computed from the background-corrected sample-in and sample-out ratio and normalized to the corresponding neutron monitor counts.

B. Scattering

The scattering measurements also used the time-of-flight technique with neutron pulses from the Ta target and the water moderator of the ORELA. Data were collected for 97 h over a two week period. The burst rate of the accelerator was 800 Hz at a power level of 10 kW and the burst width was 6.5 ns. Beam filtering to reduce the intensity of the γ flash and eliminate overlap neutrons was the same as in the transmission measurements. The neutron beam was collimated at 192 m, with both moderated and unmoderated neutrons reaching the scattering sample. The scattering sample consisted of 46.403 g of ^{52}Cr$_2$O$_3$ powder with an enrichment, in ^{52}Cr, of 99.87% poured into a 1.50-cm diameter cylinder, 2.75 cm in length. This sample was suspended within a thin-walled (0.0127 cm) cylinder of natural chromium in the center of a 1.83-m diameter evacuated scattering chamber at a distance of 200.191 ± 0.005 m from the neutron moderator. The scattering chamber was isolated from the neutron beam tube via a 0.025-cm Mylar window.

The six neutron detectors each consisted of a 4.32-cm diameter, 7.62-cm length cylinder of NE110 optically connected at each end to RCA 8850 photomultiplier tubes. These two-phototube detectors were each located 19.1 cm from the center of the scattering chamber at laboratory angles of 39°, 55°, 90°, 120°, 140°, and 160°. Each of the detectors was operated with a threshold below the single photoelectron level in a fast coincidence (between the paired phototubes) mode, with two separate pulse height spectra formed of the anode signals based on the proton recoil energy. The summed output signals from the photomultiplier pair of a given detector were processed to provide 45 000-channel time-of-flight spectra for each detector. The signal processing was configured so that only one event could be recorded in a detector, for each neutron pulse from the accelerator. The count rate of scattering events in any detector could thus never exceed the pulse rate of the accelerator. A detector was positioned in the beam during the experiment at the end of the scattering chamber to record the energy dependence of the detector efficiency and the incident flux. This spectrum was used to correct each of the scattering spectra for these combined effects. A carbon scatterer was used to intercalibrate each of the detectors and ensure uniform relative efficiencies among the detectors. Corrections were also made for the deadtime in each detector system resulting from scattering of the gamma flash, by the sample, into the detector and for a constant room background. Neither geometrical nor multiple scattering corrections were made, since the use being made of these data required only

relative cross sections. A neutron monitor detector was used to normalize each of the spectra.

III. DATA ANALYSIS

A. Transmission

The transmission data were initially averaged, appropriately preserving uncertainty information, in order to reduce the number of data points in regions between resonances that were absent of resonance structure. Sufficient data points were retained over a resonance to ensure adequate points for the broadening process while maintaining the resolution of the measurement. The resonances have been analyzed using the multilevel Reich-Moore R-matrix formalism. The transmissions are resolution broadened. These are converted to cross sections before Doppler broadening. In the latter a nuclear effective temperature of 300 K was assumed. In all of the analysis a fixed channel radius of 5.4 fm was used for ^{52}Cr. The choice of radius is arbitrary as long as it is chosen outside the range of the nuclear field. The value influences the extent of the resonance-potential scattering interference asymmetry and the R-matrix widths. Different approaches may be taken with regard to the choice of this parameter. Since this asymmetry is different for different interaction parity, one could choose radii which reproduce the observed resonance asymmetries, i.e., a different radius for each partial wave of the interaction. Two other approaches assume the same radius for all partial waves but interpret the need for differing asymmetries as indicative of corresponding differing neutron strength outside the region of analysis. One approach models this strength through a series of so-called ''poles'' or *dummy* resonances having the resonance energies (outside the analyzed energy range) and widths necessary to provide the observed resonance asymmetries via resonance-resonance interference. The other approach, and the one we have used, is to model the external strength as a logarithmic function of neutron energy as

$$R^{\text{ext}} = \alpha + \beta E - \tilde{s} \ln\left(\frac{E_{\text{up}} - E}{E - E_{\text{lo}}}\right), \tag{2}$$

where $\tilde{s}$ is the external strength and α and β are constants determined by the least-squares analysis. Our formulation permits the strength outside the region of analysis to be either uniform or a linear function of energy. In the present case we find that a uniform strength is sufficient and we have taken that strength to be equal to the strength observed within the region, for each partial wave. The resulting external R function then simply becomes an additive term in the total R function of the R-matrix formalism. This approach has been discussed elsewhere [12]. The choice of the above representation of R^{ext} is related to the ease with which we can compare the partial wave analysis with predictions of an optical model.

As mentioned earlier, under compensation of the oxygen in the sample was suggested by the quality of the R-matrix fit in regions where prominent oxygen resonances were known to occur. The extent of this under compensation was determined using a feature of the R-matrix code SAMMY [13]

TABLE I. The $^{16}O+n$ R-matrix resonance parameters used in compensating for the oxygen in the $^{52}Cr_2O_3$ transmission and scattering analyses.

Energy (keV)	J^π	Γ_n (keV)	Energy (keV)	J^π	Γ_n (keV)
−12022.000	$\frac{1}{2}^+$	9652	4312.355	$\frac{1}{2}^-$	40
−4469.500	$\frac{1}{2}^+$	5395	4467.460	$\frac{1}{2}^+$	16
434.287	$\frac{3}{2}^-$	89	4527.121	$\frac{5}{2}^+$	16
1000.256	$\frac{3}{2}^+$	201	4594.304	$\frac{7}{2}^+$	6
1309.341	$\frac{3}{2}^-$	87	4631.342	$\frac{5}{2}^-$	10
1651.380	$\frac{7}{2}^-$	16	4819.485	$\frac{3}{2}^-$	113
1688.306	$\frac{1}{2}^-$	1	5070.005	$\frac{3}{2}^+$	169
1834.118	$\frac{3}{2}^+$	15	5075.000	$\frac{9}{2}^-$	5
1901.718	$\frac{1}{2}^-$	34	5123.740	$\frac{7}{2}^-$	93
2378.170	$\frac{1}{2}^+$	162	5310.000	$\frac{1}{2}^+$	0.4
2888.700	$\frac{1}{2}^-$	0.4	5369.172	$\frac{5}{2}^+$	11
3006.900	$\frac{1}{2}^-$	0.4	5576.623	$\frac{3}{2}^-$	364
3211.757	$\frac{5}{2}^-$	5	5671.771	$\frac{5}{2}^-$	3
3290.221	$\frac{3}{2}^+$	667	5918.654	$\frac{7}{2}^+$	79
3438.400	$\frac{5}{2}^+$	2	5993.754	$\frac{3}{2}^-$	27
3441.683	$\frac{5}{2}^-$	6	6076.161	$\frac{5}{2}^-$	14
3512.603	$\frac{3}{2}^-$	1329	6087.850	$\frac{1}{2}^-$	15
3766.941	$\frac{7}{2}^-$	74	6387.658	$\frac{7}{2}^-$	40
3985.016	$\frac{1}{2}^-$	263	10674.860	$\frac{3}{2}^-$	27154
4060.227	$\frac{1}{2}^+$	108	17554.380	$\frac{3}{2}^+$	4043
4180.666	$\frac{3}{2}^+$	198	18678.560	$\frac{1}{2}^-$	26864
4303.831	$\frac{3}{2}^-$	108			

which permits searching on percentage abundances of multiple sample constituents. For purposes of this determination the most recent [14] resonance parameters for oxygen were included and held fixed in the analysis. These parameters and the spin and parity values are given in Table I. The channel radius used for the oxygen contribution to the cross section was 3.65 fm. The resonance parameters for this constituent included *dummy* resonances to represent contributions external to the region of analysis instead of the external R-function approach used in the case of the chromium contributions. This analysis indicated a sample composition of 96% chromium and 4% oxygen.

B. Scattering

The analysis of the scattering data consisted not in resonance parameter determination, but rather in the determination of spin and parity for those resonances too small to permit such assignments using the total cross section analysis techniques. Thus we have only used these data to compare with theoretical scattering predictions based upon reso-

nance parameters deduced from the total cross section analysis. The model predictions are rooted in the R-matrix formalism where the real R function is used to deduce a phase shift for a given partial wave. From these partial waves the coefficients of the Legendre expansion of the angular distributions are directly computed [15] using the FORTRAN code, RFUNC [16]. Like the transmission data, the scattering results include contributions from the oxygen in the $^{52}Cr_2O_3$ sample but unlike the transmission data, the scattering data were not compensated at all. The energy region of the analysis encompasses two broad resonances in ^{16}O with the consequence that ^{16}O contributions dominate the scattering landscape in the neutron energy ranges 400–500 keV and 900–1100 keV. We have compensated for this effect in the analysis by using the resonance parameters from Leal [14], shown in Table I, to calculate the ^{16}O scattering cross section at each angle as a function of neutron energy. These model predictions were then added to the corresponding predictions for ^{52}Cr before comparison with the $^{52}Cr_2O_3$ scattering data. This minimized the need for background and normalization corrections as the energy region was changed and ensured that resonances due to ^{16}O were not treated as background corrections.

The scattering cross section is much more sensitive to the parity of the interaction than is the total cross section with the result that unambiguous parity assignments can be made for virtually all resonances. This sensitivity derives from the fact that, for all but the smallest resonances, there is a change in resonance asymmetry as one goes from forward to backward scattering angles. The asymmetry and the change are distinctly different for even- and odd-parity resonances. To a lesser extent we can determine the total spin (J) by noting distinctions in the peak height of a scattering resonance. In the case of zero-spin target nuclei there are only two possible final spin states, for a given orbital angular momentum, which differ by the intrinsic spin of the neutron (1/2). The two analyses (total and scattering) were performed in concert. The procedure for each of the almost 300 resonances basically involved three steps: (a) assume a spin and parity for the resonance and perform a least-squares fit to the total cross section in an energy region that includes that resonance and any nearby resonances, (b) use the deduced resonance parameters to obtain the predicted scattering cross section, and (c) compare model predictions with scattering data, noting asymmetries and peak heights at different angles. For most resonances this process was repeated for $p_{1/2}$, $p_{3/2}$, $d_{3/2}$, and $d_{5/2}$ partial wave assumptions. The spin and parity assignments in Table II represent those providing the best representation of the scattering data at all angles. Since the R function involves a sum over all resonances and since resonance-resonance interference for resonances of the same spin and parity can be significant, the above procedure must be applied self-consistently among interfering resonances, involving many iterations. This study thus presents the most definitive analysis of the neutron total cross section to date over the energy range 40–1550 keV. Spin and parity values are deduced for 90% of the observed resonances below 1050 keV. Approximately 100 new resonances have been identified above that energy.

TABLE II. R-matrix resonance parameters for ^{52}Cr$+n$ in the energy range 0.040–1.05 MeV. Parentheses indicate favored J and/or π assignments. Additional resonance energies and widths above this energy range, for resonances with uncertain J^{π} assignments, have been sent to the National Nuclear Data Center (NNDC).

Energy (keV)	J^{π}	$g\Gamma_n$ (eV)	$\delta g\Gamma_n$ (eV)	Energy (keV)	J^{π}	$g\Gamma_n$ (eV)	$\delta g\gamma_n$ (eV)
48.350[a]	$\frac{3}{2}-$	8	4	346.037	$\frac{3}{2}+$	166	7
50.293	$\frac{1}{2}+$	1562	150	347.028	$\frac{3}{2}-$	673	10
57.732	$\frac{1}{2}-$	87	6	352.753	$\frac{3}{2}-$	151	6
94.950[a]	$\frac{3}{2}-$	70	35	353.376	$(\frac{3}{2})+$	70[b]	21
96.561	$\frac{1}{2}+$	6785	200	353.501	$\frac{3}{2}+$	100[b]	30
106.430[a]	$\frac{3}{2}-$	40	20	363.101[a]	$(\frac{5}{2})+$	18	9
111.800[a]	$\frac{3}{2}-$	16	8	366.963	$\frac{1}{2}+$	5035	150
121.928	$\frac{1}{2}+$	702	28	378.032	$\frac{3}{2}+$	70	5
122.972[a]	$(\frac{5}{2})+$	9	5	378.662	$\frac{1}{2}-$	439	13
130.623	$\frac{3}{2}-$	301	7	379.299	$(\frac{3}{2})+$	25	2
139.469	$\frac{1}{2}-$	167	8	386.350	$\frac{5}{2}+$	210[b]	63
140.551	$\frac{1}{2}+$	6442	190	386.550	$\frac{3}{2}+$	300[b]	90
152.921[a]	$(\frac{5}{2})+$	9	5	393.830	$\frac{3}{2}+$	94	6
177.003	$\frac{3}{2}-$	31	2	399.508	$\frac{1}{2}-$	773	23
184.841	$\frac{3}{2}+$	40[b]	12	402.803	$\frac{1}{2}+$	20763	620
184.930	$\frac{5}{2}+$	75[b]	23	403.338	$\frac{3}{2}-$	225	9
190.227	$\frac{5}{2}+$	61	4	419.814	$\frac{3}{2}+$	128	9
198.477	$\frac{3}{2}-$	66	3	422.935	$\frac{1}{2}+$	2701	110
201.058	$\frac{5}{2}+$	35	3	426.573	$\frac{3}{2}+$	171	10
231.584	$\frac{3}{2}+$	213	6	446.334	$\frac{3}{2}+$	1091[b]	327
234.971	$\frac{5}{2}+$	234	6	446.433	$\frac{3}{2}-$	125[b]	38
236.874	$\frac{1}{2}-$	1240	30	463.666	$\frac{1}{2}+$	15581	470
243.248	$\frac{3}{2}+$	80	4	468.910	$\frac{3}{2}+$	147	9
247.375	$\frac{3}{2}-$	921	2	470.077	$\frac{3}{2}-$	261	10
250.481	$\frac{1}{2}-$	504	10	471.044	$(\frac{1}{2})-$	32	3
251.515	$\frac{1}{2}+$	281	17	474.269	$\frac{1}{2}-$	135	8
258.185	$\frac{3}{2}-$	554	8	487.051	$\frac{3}{2}+$	84	6
265.120	$\frac{1}{2}+$	249	15	490.656	$\frac{3}{2}+$	413	12
283.236	$\frac{1}{2}-$	691	14	493.714	$\frac{1}{2}+$	232	15
283.773	$(\frac{5}{2})+$	19	2	501.871	$\frac{3}{2}-$	232	9
284.747	$\frac{3}{2}+$	57	3	504.323	$\frac{3}{2}+$	366	11
295.393	$(\frac{1}{2}-)$	53	3	511.820	$\frac{3}{2}-$	174	9
305.036	$\frac{5}{2}+$	440[b]	132	531.391	$\frac{3}{2}-$	319	13
305.120	$\frac{5}{2}+$	129[b]	39	533.402	$\frac{1}{2}+$	6820	200
307.265	$\frac{5}{2}+$	99[b]	30	533.931	$\frac{3}{2}+$	664	23
307.359	$\frac{5}{2}+$	160[b]	48	540.799	$\frac{5}{2}+$	804	16
311.752	$\frac{1}{2}-$	685	14	543.551	$\frac{5}{2}+$	105[b]	32
317.335	$\frac{3}{2}+$	61	4	543.806	$\frac{3}{2}-$	60[b]	18
326.209	$\frac{1}{2}+$	8555	260	553.604	$\frac{5}{2}+$	729	15
329.130	$\frac{1}{2}+$	25	5	564.032	$\frac{3}{2}-$	585	14
329.938	$(\frac{3}{2})+$	50	0	565.879	$\frac{3}{2}+$	57	5
330.125	$(\frac{5}{2})+$	167	8	570.129	$\frac{3}{2}+$	154	8
330.938	$\frac{1}{2}-$	117	6	573.498	$\frac{3}{2}-$	576	14

TABLE II. (*Continued*).

Energy (keV)	J^π	$g\Gamma_n$ (eV)	$\delta g\Gamma_n$ (eV)	Energy (keV)	J^π	$g\Gamma_n$ (eV)	$\delta g\Gamma_n$ (eV)
577.657	$\frac{3}{2}^-$	192	10	772.396	$\frac{1}{2}^+$	6119	240
580.445	$\frac{5}{2}^+$	2125	21	779.663	$\frac{3}{2}^-$	448	22
584.043	$\frac{5}{2}^+$	66	20	782.949	$\frac{5}{2}^+$	87	26
585.388	$\frac{3}{2}^+$	197	10	787.729	$(\frac{3}{2})^+$	210	13
592.077	$\frac{3}{2}^+$	346	12	795.344	$\frac{1}{2}^+$	16882	500
599.268	$\frac{3}{2}^+$	365	12	802.145	$\frac{3}{2}^+$	1499[b]	450
604.826	$(\frac{3}{2})^+$	177	11	802.285	$\frac{3}{2}^-$	271[b]	81
608.298	$\frac{3}{2}^-$	1118	22	804.361	$\frac{1}{2}^-$	717	29
613.381	$\frac{1}{2}^+$	21979	660	809.908	$\frac{5}{2}^+$	246[b]	74
613.900	$\frac{5}{2}^+$	1231	25	810.249	$\frac{3}{2}^-$	355[b]	106
618.962	$(\frac{5}{2})^+$	80	7	816.474	$\frac{1}{2}^-$	1262	50
622.704	$\frac{3}{2}^+$	319	16	822.223	$\frac{5}{2}^+$	580	23
629.991	$\frac{5}{2}^+$	683	20	842.062	$\frac{1}{2}^+$	1494	90
635.663	$\frac{3}{2}^-$	1099	22	850.385	$(\frac{3}{2})^+$	18[b]	5
638.596	$\frac{3}{2}^+$	87	7	850.670	$\frac{5}{2}^+$	281[b]	84
640.488	$\frac{5}{2}^+$	721	17	864.373	$\frac{5}{2}^+$	479[b]	144
641.862	$\frac{1}{2}^-$	493	20	866.306	$\frac{5}{2}^+$	5142[b]	1543
644.426	$\frac{3}{2}^-$	95	8	869.782	$\frac{5}{2}^+$	387[b]	116
652.009	$\frac{5}{2}^+$	92	7	870.218	$\frac{1}{2}^-$	301[b]	90
655.551	$\frac{5}{2}^+$	310	12	872.272	$\frac{3}{2}^+$	6826[b]	2048
668.547	$\frac{5}{2}^+$	105	8	872.553	$(\frac{3}{2}^-)$	84[b]	25
673.748	$\frac{5}{2}^+$	224	11	874.025	$\frac{1}{2}^+$	3556[b]	1070
674.798	$\frac{1}{2}^-$	624	25	878.970	$\frac{1}{2}^-$	2422[b]	242
679.495	$\frac{5}{2}^+$	73	7	879.265	$\frac{3}{2}^-$	1231[b]	123
685.597	$\frac{3}{2}^+$	547	16	881.823	$\frac{5}{2}^+$	941	28
687.627	$\frac{3}{2}^-$	173	10	884.984	$\frac{3}{2}^-$	688	28
693.319	$\frac{5}{2}^+$	286	11	889.149	$\frac{3}{2}^-$	1672	50
699.375	$\frac{3}{2}^+$	112	9	889.687	$\frac{1}{2}^-$	26	3
705.834	$\frac{1}{2}^-$	2920	58	892.354	$\frac{5}{2}^+$	327	20
706.324	$\frac{5}{2}^+$	1493	30	892.742	$\frac{1}{2}^+$	21196	1060
712.518	$\frac{1}{2}^+$	4973	300	900.349	$\frac{5}{2}^+$	2200	66
716.078	$\frac{3}{2}^-$	313	16	901.221	$\frac{3}{2}^-$	737	44
720.533	$\frac{3}{2}^-$	188	11	910.957	$\frac{5}{2}^+$	7758	155
721.934	$(\frac{3}{2}^+)$	87	8	912.486	$\frac{1}{2}^-$	322	26
725.716	$\frac{3}{2}^+$	332	15	918.150	$\frac{1}{2}^+$	4226	250
732.043	$\frac{1}{2}^-$	1004	30	935.379	$\frac{3}{2}^-$	1029	41
735.681	$\frac{3}{2}^+$	174	12	937.785	$\frac{1}{2}^+$	861	120
737.388	$\frac{3}{2}^+$	1365	31	939.984	$\frac{3}{2}^+$	1323	79
741.052	$\frac{3}{2}^-$	1002	30	939.997	$\frac{1}{2}^-$	981	69
740.507	$\frac{1}{2}^+$	27677	830	946.952	$(\frac{5}{2})^+$	207	17
747.352	$\frac{5}{2}^+$	3928	55	953.643	$(\frac{1}{2})^-$	186	15
758.272	$\frac{3}{2}^+$	2022	40	957.739	$\frac{5}{2}^+$	2160	43
768.064	$\frac{5}{2}^+$	227	68	960.853	$\frac{3}{2}^-$	1200[b]	360
768.765	$\frac{5}{2}^+$	919	276	961.100	$\frac{3}{2}^+$	270[b]	81

TABLE II. (*Continued*).

Energy (keV)	J^{π}	$g\Gamma_n$ (eV)	$\delta g\Gamma_n$ (eV)
961.432	$\frac{1}{2}+$	33657	2000
965.436	$\frac{3}{2}-$	321	22
970.455	$\frac{5}{2}+$	3058	61
973.053	$\frac{3}{2}+$	510	31
982.895	$\frac{3}{2}+$	679	41
986.685	$\frac{1}{2}+$	3513	280
994.147	$\frac{5}{2}+$	507[b]	152
995.191	$(\frac{1}{2})-$	754[b]	226
1001.666	$\frac{3}{2}+$	714	43
1005.656	$\frac{3}{2}-$	2478	99
1011.701	$\frac{1}{2}-$	1200[b]	360
1012.600	$\frac{5}{2}+$	1950[b]	585
1029.046	$\frac{3}{2}+$	249	22
1030.979	$\frac{3}{2}+$	309	28
1032.207	$\frac{3}{2}+$	209	21
1034.685	$\frac{5}{2}+$	4070	81
1037.372	$\frac{1}{2}+$	1555	280
1037.932	$\frac{1}{2}-$	636	38
1039.300	$\frac{3}{2}+$	214	19
1045.449	$\frac{1}{2}+$	60419	12000

[a]Seen only in scattering data.
[b]Member of a doublet.

IV. RESULTS

The total cross section data up to 1.05 MeV are shown in Fig. 1. The data uncertainties are represented as vertical lines when greater than the size of the symbol and the smooth curve represents the R-matrix parametrization of the cross section. The s-wave contribution to the total cross section is zero at the minima of the large s-wave resonances. The increase with energy of the cross section in the region of these minima reflects the increasing contribution of p-wave and higher angular momentum partial waves. At low energies the experimental cross section vanishes at these minima implying that the R^{ext} parameters for all other partial waves must be such that no model contributions result at these minima. At higher neutron energies, the need for potential scattering contributions in the region of the s-wave minima is evident and that need increases with increasing energy. This serves as one means of determining the R^{ext} parameters for the higher angular momentum partial waves.

A. General features and new findings

The large s-wave strength for this nuclide is evidenced by the broad structures located throughout the spectrum. Only 21% of the s-wave peaks have widths less than 1 keV (compared to 93% for d waves), while 28% have widths greater than 10 keV. The asymmetry of such resonances in the total cross section makes their spin determination unequivocal
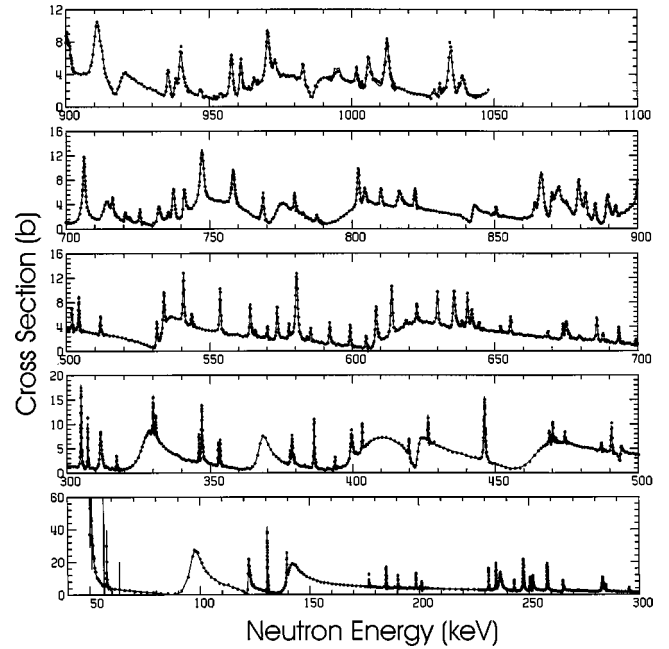

FIG. 1. Neutron total cross section for the ^{52}Cr$+n$ reaction over selected energy regions. The symbols correspond to experimental measurements and the smooth curves to R-matrix parametrization of the data. Symbols without error bars have errors less than the size of the symbols.

from the total cross section data alone for all except the resonance at 251 keV. The parity of this peak has been disputed among the various studies. It was first reported [5] as an s wave, then as $l>0$ [4], then s wave [3], then p wave [6]. With the scattering data we are able to settle the dispute, assigning it to the s-wave group. The evidence for this assignment is shown in Fig. 2 where the scattering cross sections at 90° and 160° demonstrate the absence of interference between the closely spaced resonances just above 250 keV. The differing asymmetry of even and odd parity resonances and the reversal of their asymmetry from forward to backward angles is also seen.

For the most part, resonances below 1.05 MeV are well resolved and the component spins and parities of any multiplet structures have been determined, consistent with both total and scattering cross sections. This is possible since the scattering cross sections, for all but the smallest resonances, are distinctly different for even and odd parity resonances. The resonance at 231 keV could not be simultaneously fit in totals and scattering, assuming a single resonance. Spin determination was accomplished by fitting the totals with an assumed J and then requiring the scattering peak heights to be fit by choice of spins. Above 1.05 MeV the general features of both cross sections have been qualitatively reproduced, but since all possible spin combinations have not been attempted for the multiplet structures, the parities and especially the spins have not been established. Results are thus reported here only up to 1.05 MeV for a total of 194 resonances. Between 1.05 and 1.55 MeV an additional 105 resonances have been identified. The energies of these have been transmitted to the NNDC. Rohr *et al.* [6], reported 200 resonances up to 1.0 MeV, many of which were only de-
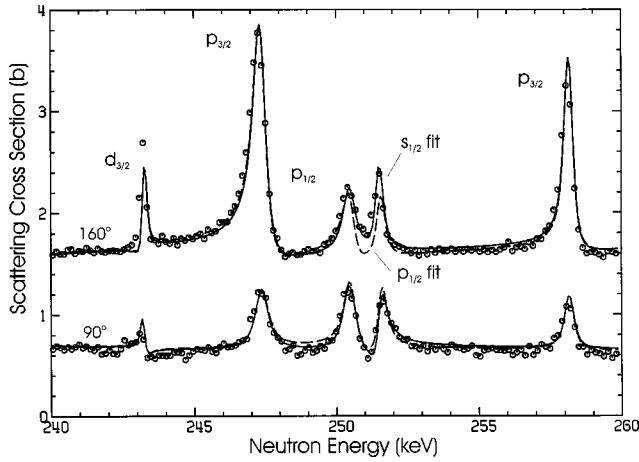
FIG. 2. Elastic-scattering cross section for the ^{52}Cr$+n$ reaction in the region of a resonance (251.5 keV) with a disputed J^π assignment. The scattering data are shown for scattering angles of 90° (bottom) and 160° (offset 1 b). The smooth curves show scattering predictions using the parameters deduced from total cross section analysis, the solid curve representing a $s_{1/2}$ assignment for the disputed resonance and the dashed curve a $p_{1/2}$ assignment. All other resonances are p waves except the first, which is d wave. Also displayed are the asymmetries for p- and d-wave scattering peaks and their asymmetry reversals between angles.
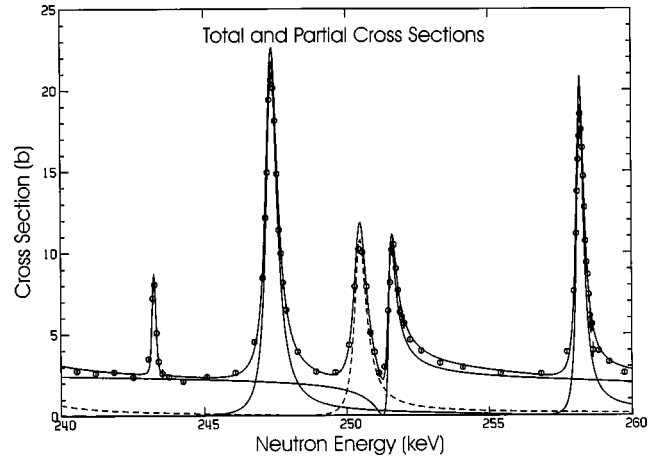

FIG. 3. Total cross section for the same energy region depicted, for scattering, in Fig. 2 showing the individual partial wave contributions to the total cross sections. The solid curves represent the total cross section and the $s_{1/2}$ and $p_{3/2}$ contributions and the dashed curve the $p_{1/2}$ contribution.

tected in their capture measurements. We have identified resonances not seen in other studies through the multiplet deconvolutions made possible by the scattering data analysis. Table II gives the deduced resonance parameters necessary to reproduce the total cross section up to 1.05 MeV. The parentheses indicate uncertainty in spin and/or parity assignment. The uncertainties for the resonance energies are approximately 0.1–0.2 %. The resonance widths uncertainties are indicated in the table of resonance parameters.

Significant differences exist between the present study and all other studies with regard to the assignment of other-than-s-wave spins and parities. This is the first work to deduce spin-separated average resonance parameters for this nuclide and to report significant strength in the d-wave channel of the interaction. Other studies have reported 12 or less d waves below 1.0 MeV. In sharp contrast we report 92. There are two good reasons to expect a large number of d waves in this nuclide: whenever the s-wave strength is large one normally expects the d-wave strength to be large and that for odd parity to be small due to the fact that the 3S size resonance peaks in the region of the minimum preceding the 3P size resonance; statistical considerations would suggest 67% more d waves than p waves. Other studies have reported d/p ratios of 0.15 or less instead of the expected 1.67. Our results yield 1.5 for this ratio, thus identifying a near-full complement of expected d-wave resonances for this nuclide. Most of the resonances which we report as due to d-wave interaction have been seen in other studies but were reported to be p waves. The parity dependence of the level spacings reported in those studies must therefore be reconsidered in light of our findings.

B. Average parameters

There are several pieces of information obtained from the resonance analysis of neutron total cross-section data. In addition to information on excited states in the compound nucleus, the energies and widths of the resonances provide for the determination of neutron strength functions and level spacings. Any nonstatistical effects may be manifest through these average features and may best be seen through plots of the cumulative number of levels or the cumulative neutron strength. We have examined such plots for each partial wave of the interaction and find no evidence for structure in any of the five interaction channels observed in this study. In subsections below we present plots for selected angular momenta to indicate the uniform nature of these trends.

Another feature obtained from the analysis is the contribution to the background cross section from any strength outside of the region of analysis. This R^{ext} contribution increases with energy for a given angular momentum. At a given energy it is less significant for increasing angular momentum of the interaction. Generally speaking, s-wave resonances provide the dominant contribution as shown in Fig. 3. Figure 4 in Ref. [7] and discussions in Sec. V will give some idea of the trends of these contributions to the underlying total cross section.

The level spacings, strength functions and the R^{ext} have been deduced for all individual partial waves up to and including $d_{5/2}$ and are presented in Table III. The latter feature is characterized by the constants α, β, and the R-matrix strength, as discussed in Sec. III.

1. Average level spacings

The number and distribution of s- and p-wave levels observed in this study are shown by the histograms in Fig. 4. This figure is to be compared with Figs. 3 and 5 in Ref. [6] where observed gaps were noted in the s-wave level density at energies centered near 200 and 700 keV and a sharp discontinuous increase in the p-wave level density was seen
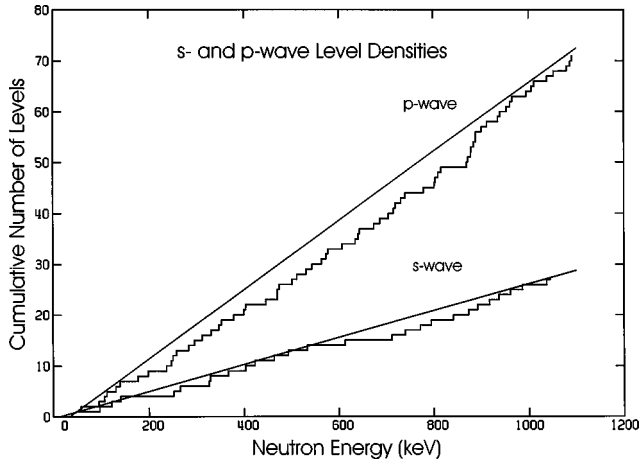
FIG. 4. The number of s and p levels (histograms) observed in the ^{52}Cr$+n$ reaction. The lines are calculated from the average level spacings. The ratio of their slopes (2.6) is in good agreement with that expected from statistical considerations.

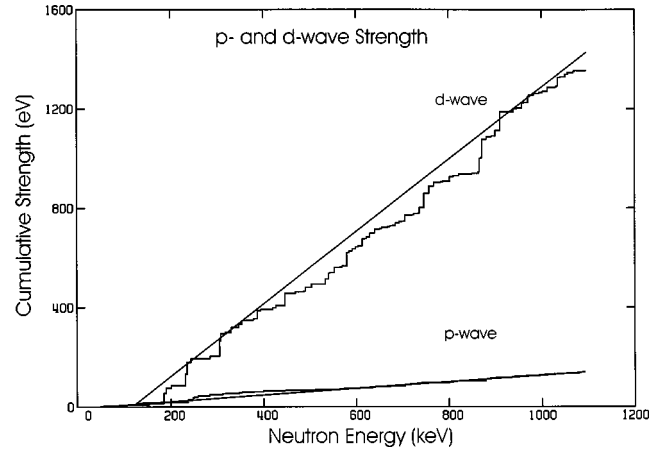FIG. 5. The cumulative neutron strength (histograms) for p- and d-wave channels in the ^{52}Cr$+n$ reaction. The slopes of the lines are related to the corresponding strength functions.

near 250 keV. The newly identified s-wave resonance at 250 keV somewhat weakens the case for doorway structures in the s-wave channel by narrowing one of those gaps. Our identification of many of the previously determined p waves as d-wave resonances completely removes their reported [6] ''clustering'' of p waves at 250 keV and thus casts doubt upon the conjecture that fragmentation into more complicated states was responsible. Moreover, the firm parity determinations presented here result in a s/p level spacing ratio (2.6 ± 0.3) that is consistent with the statistical expectation (3), contravening the proposed nonstatistical effects suggested by their ratio of 7.8 above 250 keV. Since similar plots for d-wave resonances and for all partial wave components are also very uniform over the entire energy range of analysis, it would seem that this nuclide is absent of nonstatistical effects.

2. Strength functions

Our s- and p-wave strength functions and level spacings are in agreement with values reported by Mughabghab [17]. However, for p waves our disagreement with two similar studies [3,6] is outside uncertainties. This is due, as mentioned above and discussed below, to their misassignment of d-wave resonances as p waves. The uniformity of strength

for both odd and even angular momentum interactions is seen in Fig. 5 where we have plotted the cumulative strength for p and d waves. Also seen is the very different strengths for these two components of the interaction. Ours is the first work to report average parameters for d waves, based upon resonance analysis. The strength function we obtain is lower than predictions [18] by a factor of 2 but is consistent with trends in the experimental values reported by Mughabghab [17]. A uniformity similar to that for p and d waves is seen in the neutron strength for the s-wave interaction channel and in all partial wave channels up to and including $d_{5/2}$, thus reshaping the previously posited nonstatistical nature of the neutron interaction for this nuclide.

V. DISCUSSION

Since one motivation of this study was to resolve the differences among the cross sections of evaluated data sets, any discussion must include major contrasts between this and other relevant, similar studies. The density of levels in ^{52}Cr available to neutrons with energies up to 1 MeV is such that differences in resolution for the 200- and 400-m measurements is unimportant. We observe all but three of the resonances reported from the 400-m data. One surprising difference was noted among the studies, for deduced resonance widths, which could partially explain the differences in the predicted cross section at low neutron energies. This is shown in Table IV where we have included just the widths of large s-wave resonances which influence the cross section beyond their immediate extent.

Despite the agreement of reported s-wave strength functions, there are clearly systematic discrepancies among the reported resonance widths [3,6], one group reporting generally larger widths at low energies and smaller widths at higher energies, the differences being as large as 100%. Our results tend to lie intermediate to those of these two investigations. Given the extent of contributions of large s-wave resonances beyond their own proximity, consequent differences in the predicted total cross section between resonances would be expected and can also measurably influence the

TABLE III. Average resonance parameters for ^{52}Cr$+n$.

lJ	Number of resonances	$\langle D_{lJ}\rangle$ (keV)	S_{lJ} ($\times10^4$)	α_{lJ}	β_{lJ} (MeV)$^{-1}$	$\tilde{s}_{lJ}$
$s_{1/2}$	28	37(4)[a]	3.5(10)	$-0.010(4)$	0.22(2)	0.13(4)
$p_{1/2}$	27	38(4)	0.7(2)	$-0.18(2)$	0.07(2)	0.029(9)
$p_{3/2}$	40	25(2)	0.33(8)	$-0.15(2)$	0.13(2)	0.014(3)
$d_{3/2}$	49	18(1)	2.9(6)	0.0	0.0	0.12(3)
$d_{5/2}$	50	19(1)	2.9(6)	0.0	0.0	0.13(3)
p	67	15(1)	0.44(8)			
d	99	9.4(5)	2.9(4)			

[a]In our notation 37(4) means 37 ± 4, etc.

TABLE IV. Comparison of s-wave resonance widths, Γ_n, deduced in three comparable studies of $^{52}Cr+n$. Energies and widths are in units of keV.

Energy	Γ_n [a]	$\delta\Gamma_n$	Γ_n [b]	$\delta\Gamma_n$	Γ_n [c]	$\delta\Gamma_n$
50.3	1.5	0.15	1.6	0.06	1.8	0.09
96.6	6.8	0.26	8.0	0.9	7.5	0.15
140.5	6.4	0.20	7.0	0.9	5.2	0.5
326.2	8.6	0.26	10.0	0.5	7.5	0.3
367.0	5.0	0.15	6.5	0.4	4.3	0.1
402.8	20.8	0.62	30.0	3.0	15.0	1.0
463.7	15.6	0.47	15.0	1.5	6.8	0.3
533.4	6.8	0.21	5.3	0.5	4.8	0.1
613.5	22.0	0.66	16.0	2.0	35.0	3.0
712.5	5.0	0.30				
740.7	27.7	0.83	30.0	3.5	40.0	3.0
772.4	6.1	0.24	5.8	0.6	8.0	0.8
795.4	16.9	0.51	14.4	1.5	30.0	3.0
874.0	3.6	1.1	6.0	1.2		
892.8	21.2	1.04	1.0	0.3		
918.1	4.2	0.25	5.0	1.0		
961.4	33.7	2.02	23.4	4.5		

[a]Present study.
[b]Reference [6].
[c]Reference [3].

predicted off-resonance cross section at low neutron energy. This could be in part responsible for differences reported [8] in this quantity among several evaluated data files (ENDF/B-6, JEF-2, and JENDL-3). The difference in predicted low-energy cross sections resulting from the discrepant resonance widths noted in Table IV can be as much as 0.25 b.

We have found other factors, however, that would result in larger differences in the evaluated cross sections, if neglected. One of the evaluations is based upon resonance parameters which were deduced from the fitting of different energy regions by varying both the channel radii and the parameters of *dummy* resonances to give the best fit for that region, with different radii and parameters resulting for different energy regions [3,19]. Since these so-called ''external contributions'' can contribute significantly to the off-resonance cross section, this procedure frustrates the need to provide a unified, consistent description of these influences throughout the analysis region. We take the approach of using the same radius (5.4 fm) for all partial waves and for the entire analysis, incorporating as a part of the R function a contribution due to the combined effect of all external resonances [7,12]. This is done in a single logarithmic function of energy for each partial wave instead of using a set of *dummy* resonances with energies outside the range of analysis. This external R function produces a characteristic resonance-potential scattering interference for each partial wave, which is manifested in a characteristic resonance asymmetry (see Fig. 3) for all resonances of that group. The shape of this function then becomes a parameter in the description of the cross section and is equivalent to the use of *dummy* resonances with energies above and/or below the region of analysis. In one of the data sets, *dummies* were used

TABLE V. Comparison of partial-wave cross sections to evaluated discrepancies, ($\delta\sigma$). The energy ranges are in keV and the cross sections are in barns.

Energy range	$\sigma(p_{1/2})$	$\sigma(p_{3/2})$	$\delta\sigma$
50–100	0.03	0.0	1.0
100–200	0.15	0.0	0.15
200–500	0.45	0.1	0.3
500–1000	0.5	0.2	0.3

only for s waves [6] and in another study [3] no potential scattering influences were reported with the resonance parameters, for any partial waves. A characteristic feature of model cross sections which have not incorporated this important influence for the non-s-wave components will be the under prediction of the s-wave minima and maxima by similar amounts. The detail of the cross-section fits published earlier is not sufficient to be certain but there are indications that this was a problem for both the 80-m and the 400-m measurements. In the former, no external contributions were reported and in the latter only s-wave contributions were reported. This deficiency may be corrected in a very natural way by the inclusion of p-wave potential scattering in the description of external contributions. The need for this contribution is strengthened and corroborated by the fact that the external contribution needed to provide for the above deficiency in the off-resonance cross section simultaneously provides for the observed asymmetry in the p-wave resonance shapes through resonance-potential scattering interference for that partial wave. In the present study this contribution to the background cross section due to p waves is seen in Table V which gives the contributions due to each p-wave component at selected energy ranges over the analyzed region together with the maximum discrepancy reported between the average cross sections of the evaluated data sets [8]. The importance of this effect, for a given partial wave, depends upon the proximity of a given mass nucleus to a size resonance corresponding to the same angular momentum. For ^{52}Cr, near the $3S$ resonance, the contribution from p waves is small while for ^{86}Kr, near the $3P$ resonance, this is an important effect.

Differences among the studies, for the other properties typically reported in total cross section analyses, are seen in Table VI. While these differences are outside the uncertainties for the p and d waves, these differences will not signifi-

TABLE VI. Comparison of average resonance parameters from present and comparable studies.

		Present		Rohr		Agrawal	
		$\langle D_{lJ}\rangle$	S_{lJ}	$\langle D_{lJ}\rangle$	S_{lJ}	$\langle D_{lJ}\rangle$	S_{lJ}
l	N	(keV)	($\times10^4$)	(keV)	($\times10^4$)	(keV)	($\times10^4$)
s	28	37(4)[a]	3.5(10)	43.4(47)	2.9(9)	45.(6)	3.(1)
p	67	15(1)	0.44(8)	7.5(3)	0.67(9)	9.0(7)	0.95(10)
d	99	9.4(5)	2.9(4)	62(10)	1.36(4)		

[a]In our notation 37(4) means 37 ± 4, etc.

cantly affect the evaluated average total cross section. As shown, our results are very different for the *p*- and *d*-wave average parameters because of the very different number of resonances in each spin group. In previous studies most resonances were assigned as *p* waves based upon resonance shapes observed in the total cross section, contrary to expectations based upon statistical considerations. However, the neglect of *p*-wave potential scattering can significantly impact *p*-wave resonance shapes and thus the parity assignments consequently deduced. Our scattering results conclusively establish that many of the resonances previously assigned as *p* waves are definitely *d* waves and thus account for the differences in average parameters for these partial waves. Since Rohr reported results for selected energy segments, and not over the entire energy range, we have taken their resonance parameters and performed the usual calculations of the strength functions to complete this table, for the *p*- and *d*-wave results. The number of resonances shown correspond to the present study. By comparison, Rohr's study revealed 133 *p* waves and 12 *d* waves.

VI. CONCLUSION

The present study has not added significantly to the number of resonances observed below 1 MeV but has determined the spins and parities for more than 90% of those observed using analysis procedures that included both total and elastic-scattering cross-section data. As a result, previous claims of parity dependence for the level density and the nonstatistical character of the interaction are brought into question by our results. Many of the resonances previously attributed to *p*-wave interaction have been shown to result from *d*-wave interaction, with a consequent decrease in the *p*-wave strength and increase in *d*-wave strength in this nuclide. We have not yet completed J^{π} assignments for resonances beyond the 1.05 MeV neutron energy due to the multiplet complexities resulting from the need for increased energy resolution. Only approximate energies have been determined for these resonances and they are thus not included in the table of resonance parameters, but have been sent to the NNDC. The treatment of the influences, within the analyzed region, due to strength outside has been shown to be an important factor in any accurate analysis of the data. This feature of the analysis has been largely ignored in previous studies, at least for the *p*-wave channel. We have found this to provide non-negligible contributions to the predicted off-resonance background cross sections. The data cannot be properly represented without it. This would appear to be the primary reason for discrepancies among the various evaluated data sets above 500 keV neutron energy. Below that energy we can only point to the discrepant *s*-wave neutron widths reported in earlier studies and suggest that our parameters would better represent the cross section because of our unified and consistent treatment of external influences and resonance asymmetries throughout the energy region of the analysis.

[1] B. J. Allen and R. de L. Musgrove, in Proceedings of the Geel Conference on Neutron Data of Structural Materials for Fast Reactors, 1977, p. 447.

[2] C. D. Bowman, E. G. Bilpuch, and H. W. Newson, Ann. Phys. (N.Y.) **17**, 319 (1962).

[3] H. M. Agrawal, J. B. Garg, and J. A. Harvey, Phys. Rev. C **30**, 1880 (1984).

[4] I. A. Korzh, V. A. Mishchenko, E'. N. Mozhzhukhin, and N. M. Pravdivyi, Yad. Fiz. **35**, 1097 (1982) [Sov. J. Nucl. Phys. **35**, 641 (1982)].

[5] H. Beer and R. R. Spencer, Nucl. Phys. **A240**, 29 (1975).

[6] G. Rohr, R. Shelley, A. Brusegan, F. Poortmans, and L. Mewissen, Phys. Rev. C **39**, 426 (1989).

[7] R. F. Carlton, R. R. Winters, C. H. Johnson, N. W. Hill, and J. A. Harvey, Phys. Rev. C **38**, 1605 (1988).

[8] M. Salvatores, in *Proceedings of the International Conference on Nuclear Data for Science and Technology*, Julich, 1991, edited by S. M. Qaim (Springer-Verlag, New York, 1992), p. 17.

[9] D. C. Larson (private communication).

[10] D. C. Larson, N. M. Larson, J. A. Harvey, N. W. Hill, and C. H. Johnson, Oak Ridge National Laboratory Report No. ORNL/TM-8203, Oak Ridge, Tennessee, 1984 (unpublished).

[11] D. C. Larson, N. M. Larson, and J. A. Harvey, Oak Ridge National Laboratory Report No. ORNL/TM-8880, Oak Ridge, Tennessee, 1984 (unpublished).

[12] C. H. Johnson, C. Mahaux, and R. R. Winters, Phys. Rev. C **32**, 359 (1985); C. H. Johnson and R. R. Winters, *ibid.* **21**, 2190 (1980).

[13] N. M Larson, Updated Users Guide for SAMMY: Multilevel R-Matrix Fits to Neutron Data Using Bayes Equations, ORNL/TM-9179/R4, Oak Ridge National Laboratory, 1998.

[14] L. C. Leal, R. O. Sayer, N. M. Larson, and R. R. Spencer, Trans. Am. Nucl. Soc. **79**, 175 (1998).

[15] Meier *et al.*, Helv. Phys. Acta **27**, 577 (1954); J. M. Blatt and L. C. Biedenharn, Rev. Mod. Phys. **24**, 258 (1952).

[16] F.G. Perey, RFUNC-A Code to Analyze Differential Elastic Scattering Data, ORNL/TM-1112, Oak Ridge National Laboratory, 1989.

[17] S. F. Mughabghab, M. Divadeenam, and N. E. Holden, *Neutron Cross Sections* (Academic, New York, 1981), Vol 1.

[18] M. Divadeenam, Ph.D. thesis, Duke University, 1967.

[19] A. Brusegan *et al.*, in *Proceedings of the International Conference on Nuclear Data for Basic and Applied Science*, Santa Fe, 1985, edited by P. G. Young *et al.* (Gordon and Breach, New York, 1986), Vol. 2, p. 633.